CHAPTER VI

WIRELINE FORMATION TEST IN SINGLE LAYER RESERVOIR WITH INVADED ZONE

A single layer reservoir with an invaded zone due to mud filtrate is investigated to evaluate the effect of mobility ratio and effects of radius of invasion. The reduction in permeability of a zone around the well causes the skin effect. Simulations and interpretations are performed under different scenarios to see whether wireline formation testing with a single probe can be used to evaluate reservoir properties of an invaded reservoir. The grid sizes of the reservoir model are the same as those in the base case and so are the reservoir conditions and fluid properties. The reservoir model has two zones as shown in Figure 6.1. The permeability anisotropy ratio, k_v/k_h, for both invaded zone and uninvaded zone are kept constant at 0.1. In this section, three different sets of damaged and undamaged permeability are used. In each case set, the effects of mobility ratio and effects of radius of invasion are studied.

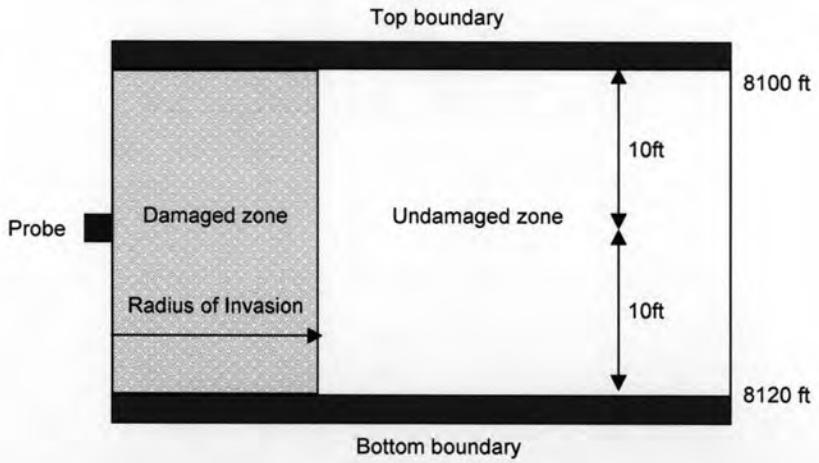

Figure 6.1 : Schematic reservoir description for invaded reservoir.

6.1 Case I : Undamaged Permeability of 50 mD, Damaged Permeability of 25 mD

6.1.1 Effects of Mobility Ratio

In this case study, the objective is to investigate the effects of mobility ratio between invaded zone and the reservoir on pressure transients by fixing the permeability of the undamaged zone while varying the permeability of the damaged zone. Here, we assume the viscosity of the fluid in the invaded zone is the same as that in the reservoir. Three different mobility ratios, K_{hi}/K_{hu} of 0.3, 0.5, and 0.8 are considered. The undamaged permeability is fixed at 50 mD while the damaged permeability varies with the mobility ratio. The radius of invasion is fixed at 1.2867 ft. away from the borehole wall as shown in Figure 6.2. The flow period consists of a 30-minute drawdown and a 90-minute buildup. After running reservoir simulation for pressure response, the data were then interpreted by pressure transient analysis technique. The pressure history and the diagnostic plots of the tests are shown in Figures 6.3 and 6.4, respectively, and the interpreted results are tabulated in Table 6.1. The regression fits to the tests are shown in Appendix B.

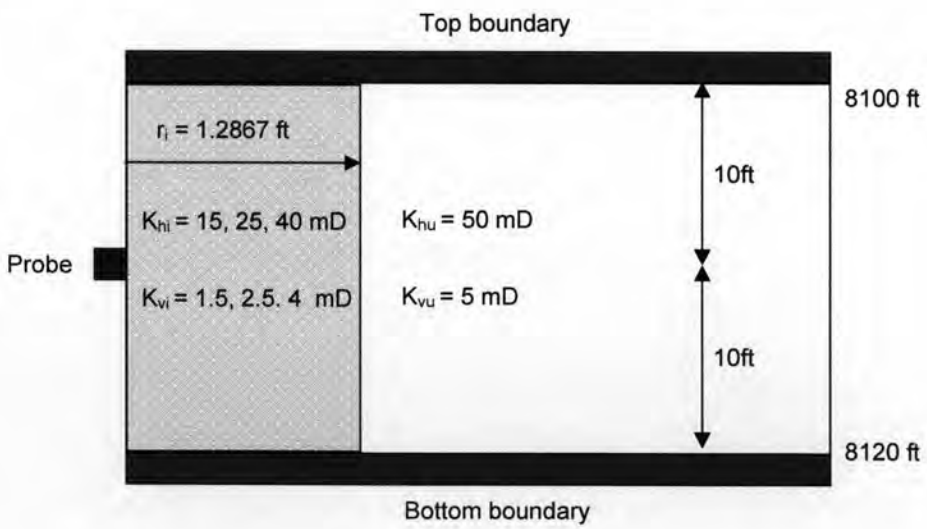

Figure 6.2 : Schematic reservoir description for different mobility ratios between invaded zone and uninvaded reservoir for case I.

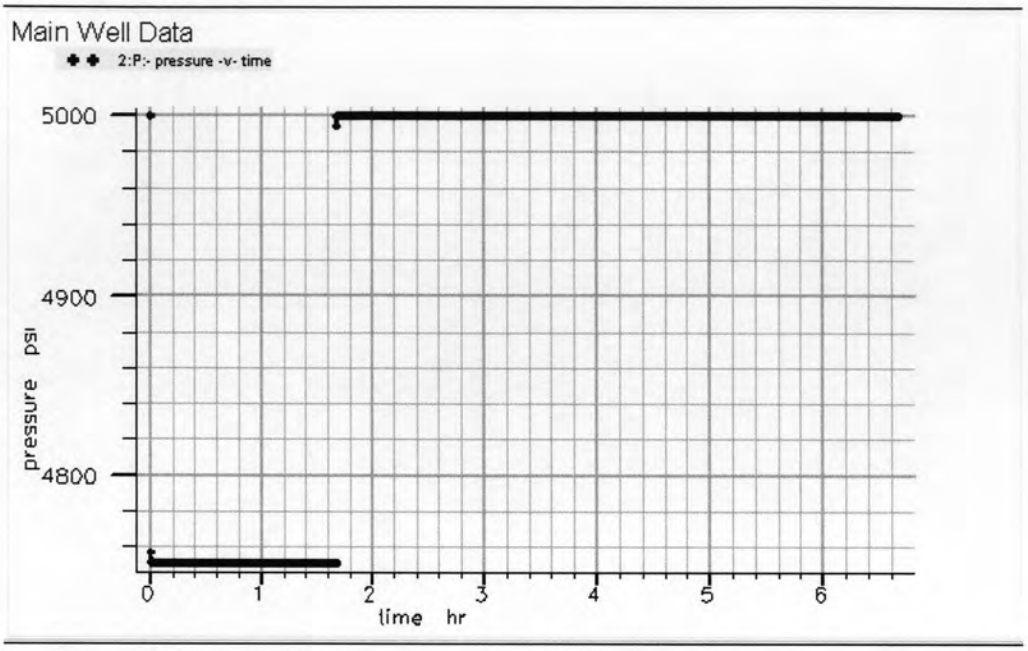

Figure 6.3 : Pressure history of case K15-50 (mobility ratio = 0.3)

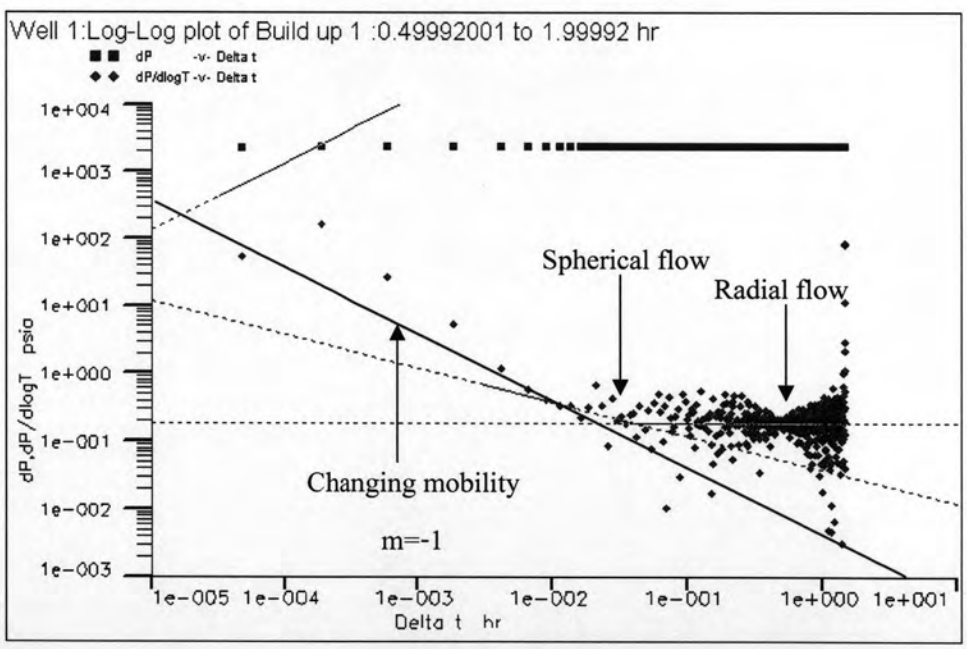

(a) Mobility ratio = 0.3

Figure 6.4 : Diagnostic plots for different mobility ratios between invaded zone and uninvaded reservoir for case I.

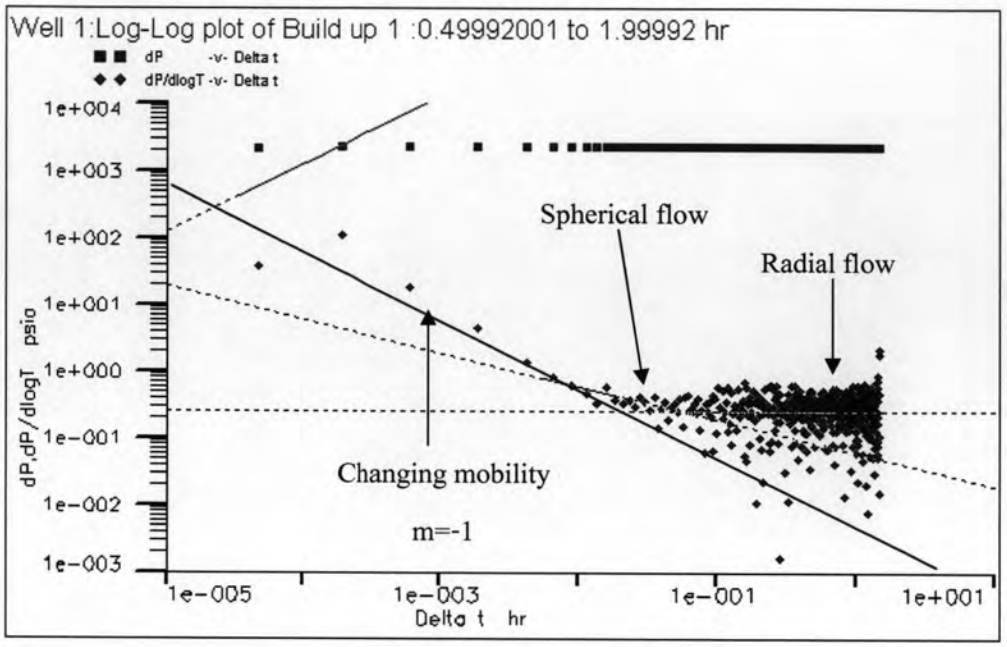

(b) Mobility ratio = 0.5

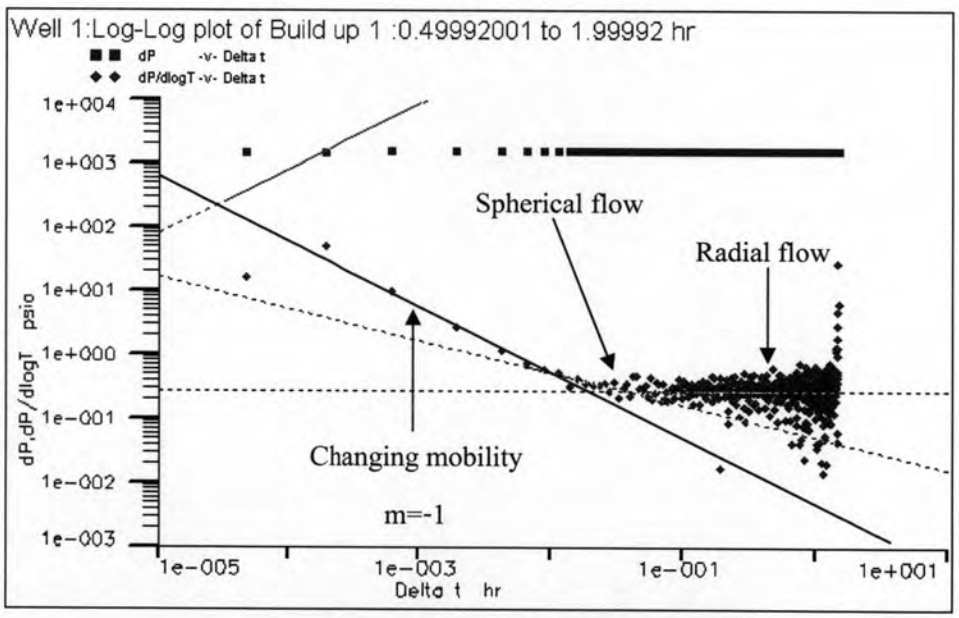

(c) Mobility ratio = 0.8

Figure 6.4 : Diagnostic plots for different mobility ratios between invaded zone and uninvaded reservoir for case I (continued).

Table 6.1 : Interpreted results for different mobility ratios between invaded zone and uninvaded reservoir for case I.

Case	K_{hi} (mD)	K_{hu} (mD)	S_P	S_M	S_t	Interpreted results		Error %		
						K_h (mD)	Skin	K_h (mD)	S_M	S_t
K15-50	15	50	1.97	3.823	5.793	48.4	5.198	-3.2	35.97	-10.27
K25-50	25	50	1.25	1.638	2.888	48.6	2.499	-2.8	52.56	-13.46
K40-50	40	50	0.84	0.409	1.249	47.7	1.091	-4.6	166.7	-12.65

As can be seen in Figure 6.4 (a), (b), and (c), the derivatives in the diagnostic log-log plot are scattered due to numerical error from reservoir simulation. The scattering of the derivative can be reduced by data filtering or smooth options available in the well test analysis software. The smoothed diagnostic plots are shown in Figure B1 (a), (b), and (c) in Appendix B.

In this case study, we fixed the radius of invasion but varied the permeability in the damaged zone. The effect from the permeability contrast between the native reservoir and the damaged zone can be quantified by skin factor. The interpreted results obtained from the regression for different mobility ratios are summarized in Table 6.1. S_P, S_M, and S_t stand for probe skin, mechanical skin, and total skin, respectively. The probe skin is estimated by interpreted the pressure response simulated from homogeneous reservoir with the invaded zone permeability. The mechanical skin is calculated from the definition of skin factor due to damage, and the total skin is the mechanical skin added with the skin due to probe. In cases K15-50, K25-50, and K40-50, the interpreted skin factor is different from the mechanical skin factor, with an error of 35.97, 52.56, and 166.7 %, respectively. It can be seen that the interpreted skin factor is too high compared with the mechanical skin factor but if we compare the interpreted skin with the total skin, the errors are not that high. It can be concluded that the interpreted skin factor is affected by the spherical skin (skin due to probe) because our reservoir model is single probe flow model. For horizontal permeability, the interpreted results are quite similar to the undamaged zone permeability.

For this case study, a negative unit slope indicating the changing in mobility cannot be seen clearly. Since, the radius of invasion is too small, the changing in mobility can be affected by wellbore storage effect and the spherical flow regime.

As can be seen in Figure B1 in Appendix B, the regression plot of high mobility ratio (case K40-50) shows good consistency on the diagnostic plot more than that of low mobility ratio (cases K15-50 and K25-50). Thus, the regression with vertical interference model can be used very well for high mobility ratio but can be moderately applied for low mobility ratio.

6.1.2 Effects of Radius of Invasion

In this case study, the objective is to investigate the effects of radius of invasion on pressure transients by fixing the permeability of the damaged and the undamaged zone while varying the radius of invasion as depicted in Figure 6.5. Six different radii of invasion, r_s of 0.44, 0.64, 1.28, 3.35, 4.56, and 6.19 ft. are considered. The undamaged permeability is fixed at 50 mD, and the damaged permeability is fixed at 25 mD. The flow period consists of a 30-minute drawdown and a 90-minute buildup. After running reservoir simulation for pressure response, the data were then interpreted by pressure transient analysis technique. The pressure history and the diagnostic plots of the tests are shown in Figures 6.6 and 6.7, respectively, and the interpreted results are tabulated in Table 6.2. The regression plots of the tests are shown in Appendix B.

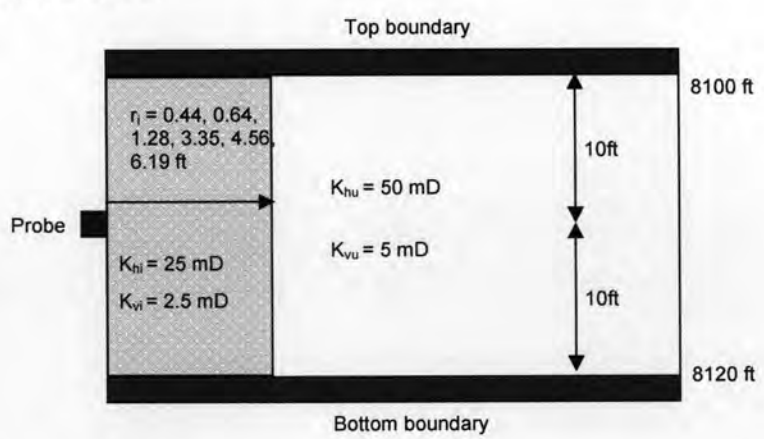

Figure 6.5 : Schematic reservoir description for different radii of invasion for case I.

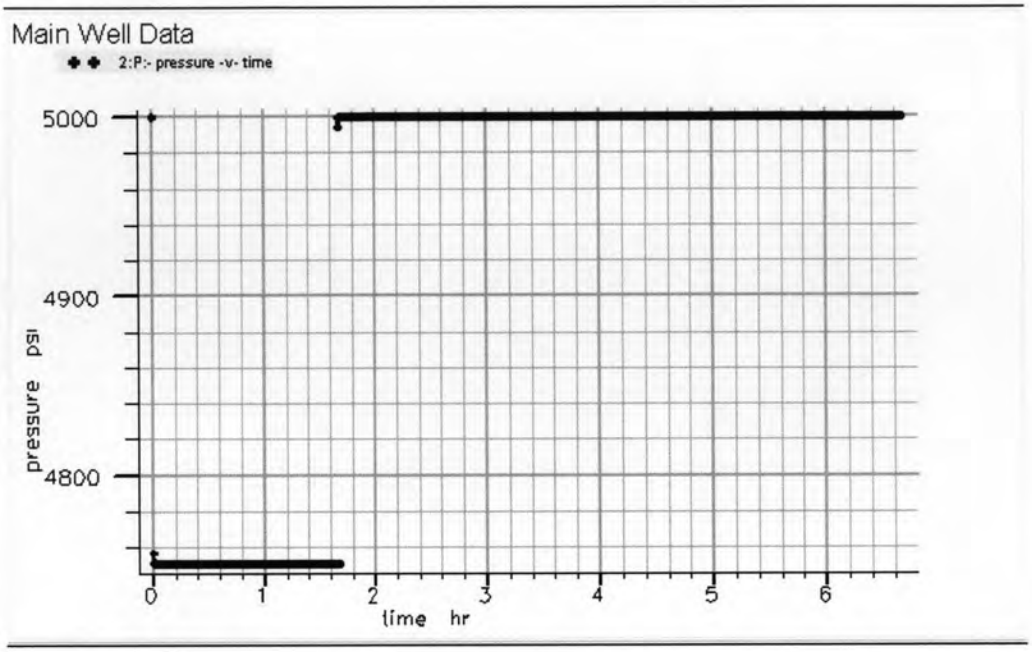

Figure 6.6 : Pressure history of case K25-50-3 (radius of invasion = 1.28 ft.)

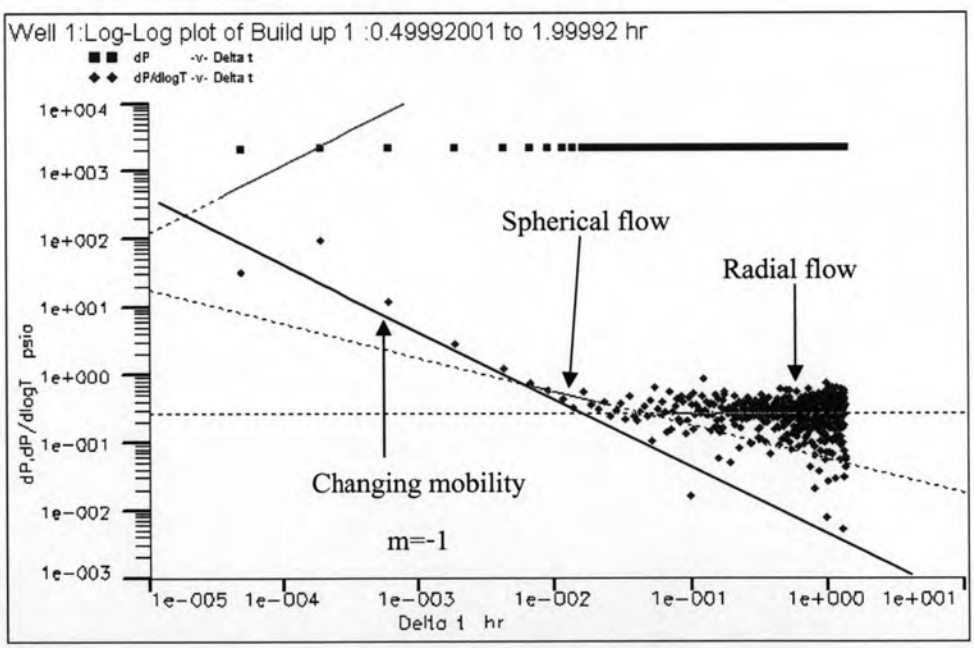

(a) Radius of Invasion = 0.44 ft.

Figure 6.7 : Diagnostic plots for different radii of invasion for case I.

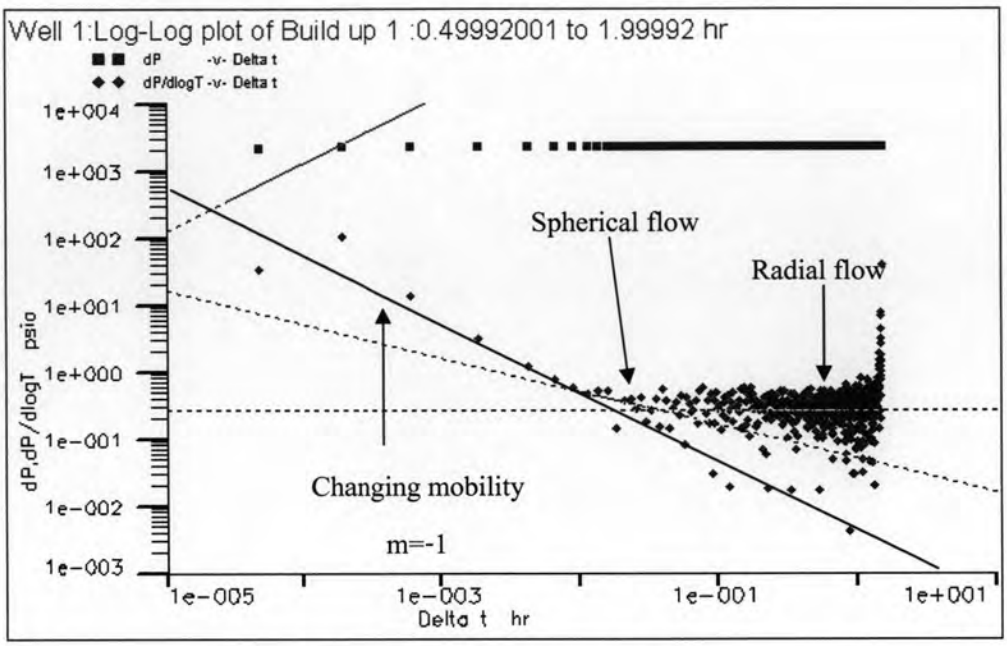

(b) Radius of Invasion = 0.64 ft.

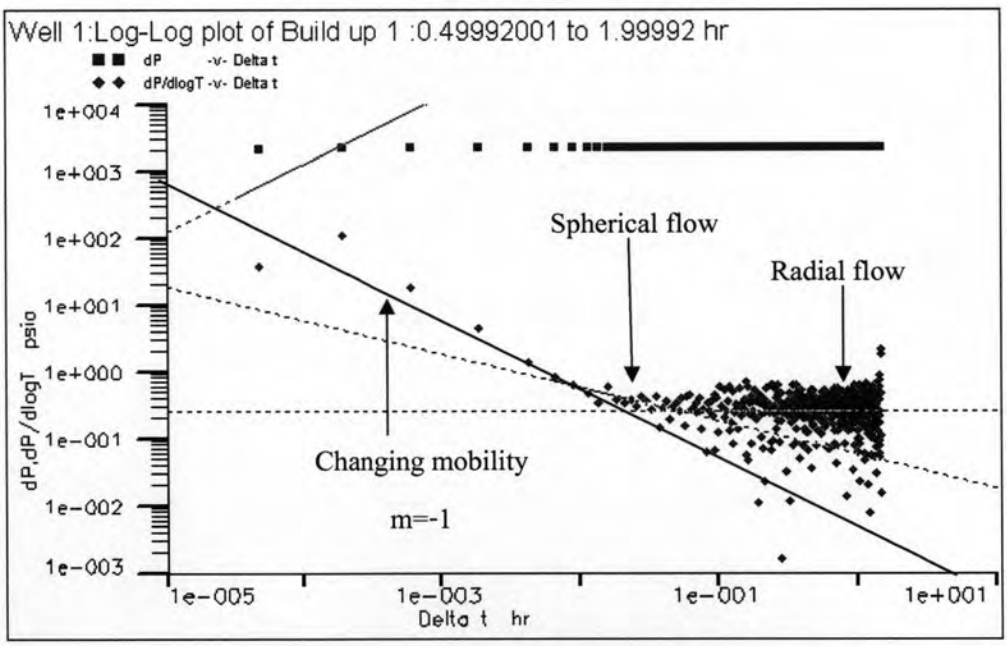

(c) Radius of Invasion = 1.28 ft.

Figure 6.7 : Diagnostic plots for different radii of invasion for case I (continued).

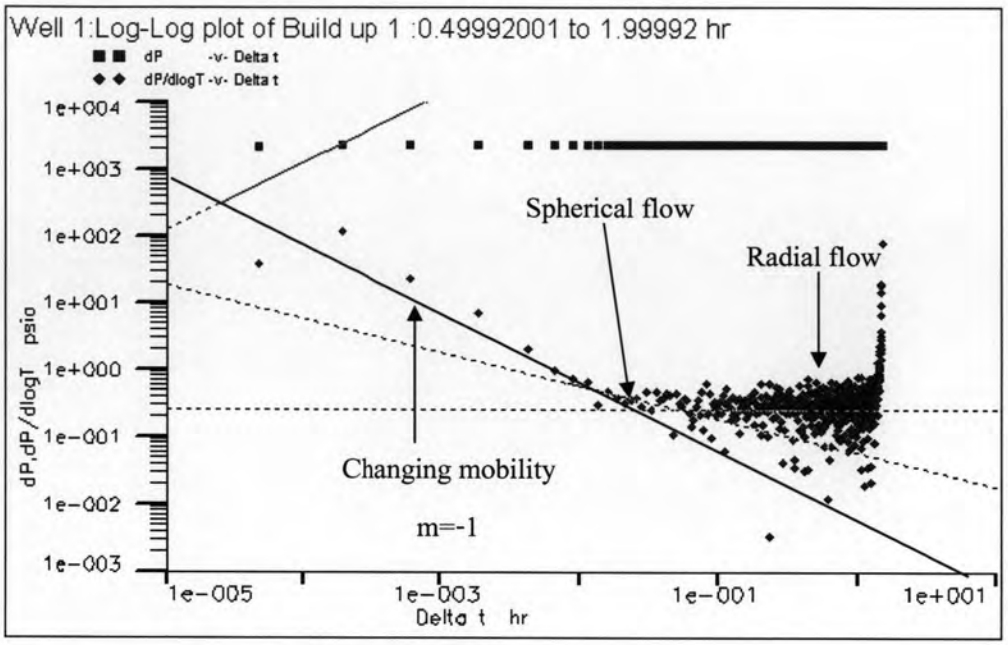

(d) Radius of Invasion = 3.35 ft.

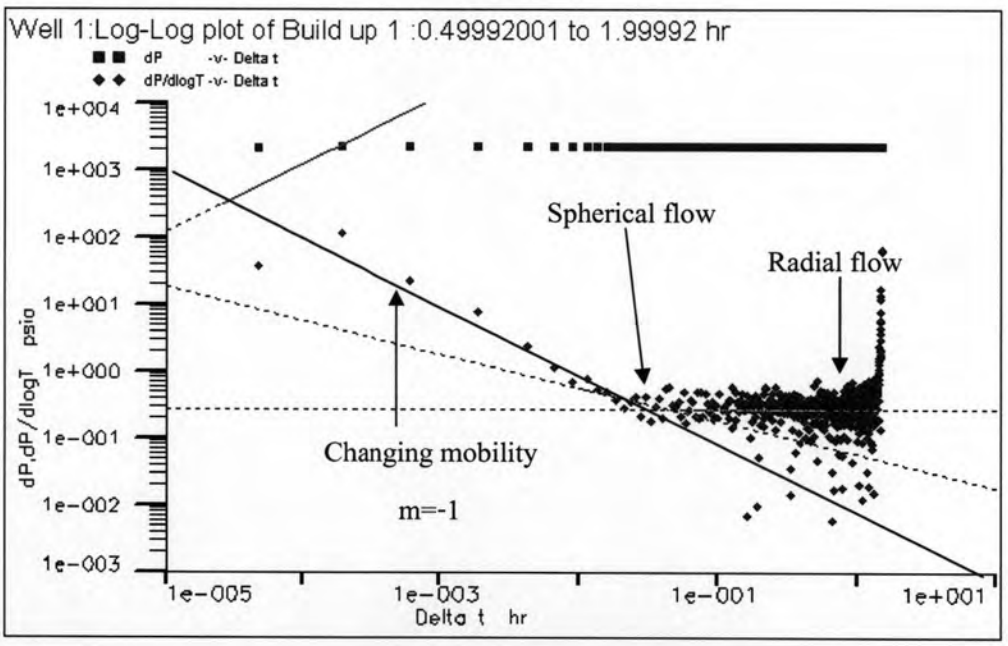

(e) Radius of Invasion = 4.56 ft.

Figure 6.7 : Diagnostic plots for different radii of invasion for case I (continued).

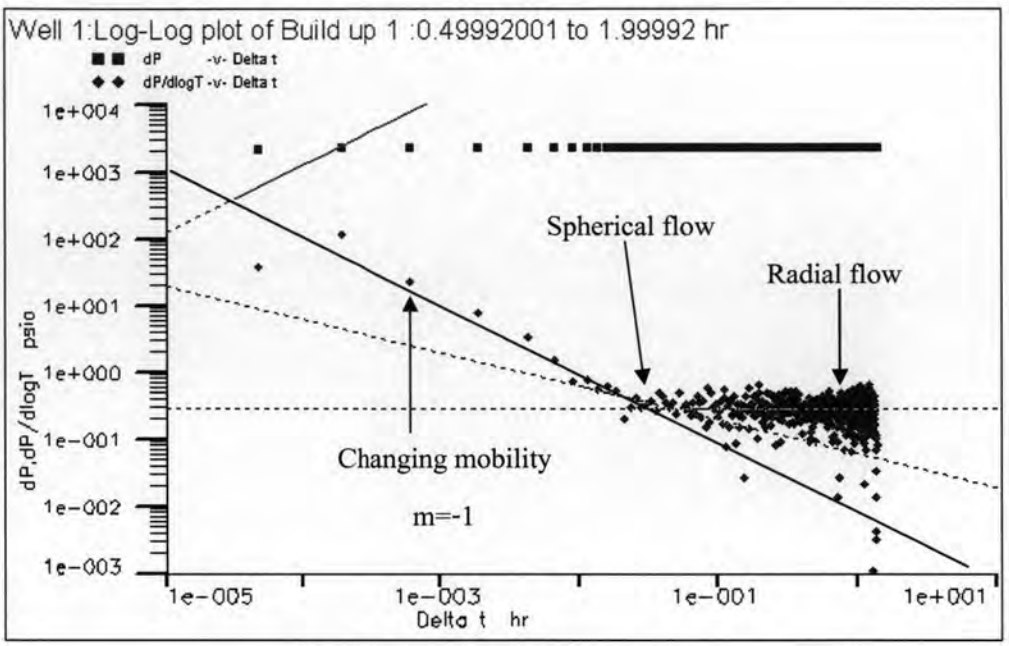

(f) Radius of Invasion = 6.19 ft.

Figure 6.7 : Diagnostic plots for different radii of invasion for case I (continued).

Table 6.2: Interpreted results for different radii of invasion for case I.

Case	r_s (ft)	K_{hi} (mD)	K_{hu} (mD)	S_p	S_M	S_t	Interpreted results		Error %		
							K_h (mD)	Skin	K_h (mD)	S_M	S_t
K25-50-1	0.44	25	50	1.25	0.569	1.819	49.9	2.084	-0.20	266.25	14.56
K25-50-2	0.64	25	50	1.25	0.947	2.197	48.7	2.188	-2.60	131.04	-0.41
K25-50-3	1.28	25	50	1.25	1.638	2.888	48.6	2.583	-2.80	57.52	-10.56
K25-50-4	3.35	25	50	1.25	2.595	3.845	48.7	2.998	-2.60	15.52	-22.02
K25-50-5	4.56	25	50	1.25	2.904	4.154	49	3.098	-2.00	6.68	-25.42
K25-50-6	6.19	25	50	1.25	3.210	4.46	51.7	3.117	3.40	-2.89	-30.11

As can be seen in Figure 6.7 (a)-(f), the derivatives in the diagnostic log-log plot are scattered due to numerical error from reservoir simulation. The scattering of the derivative can be reduced by data filtering or smooth options available in the well test analysis software. The smoothed diagnostic plots are shown in Figure B2 (a)-(f), in Appendix B.

In this case study, we fixed the permeability of damaged and undamaged zone but varied the radius of invasion in the damaged zone. The interpreted results obtained from the regression for different radii of invasion are summarized in Table 6.2. It can

be seen that the interpreted skin factors for cases K25-50-1, K25-50-2, K25-50-3, K25-50-4, and K25-50-5 are overestimated compared with the mechanical skin factor, S_M. This is due to the fact that the interpreted skin factor is affected by the spherical skin or the skin due to probe, S_P as can be seen that the errors between the interpreted results and the total skin factor, S_t are reduced. For cases K25-50-4, K25-50-5, and K25-50-6 which have large radius of invasion, the interpreted skin factor is different from the total skin factor, with an error of -22.02, -25.42, and -30.11 %, respectively. The errors are large because when the radius of invasion goes further into the reservoir, the reservoir behaves like a composite reservoir. But our regression model used is simple vertical interference test model. Therefore, the skin factor could not be accurately estimated if the radius of invasion is too large. A better estimation for the skin can be achieved with a composite reservoir model with single probe which is not currently available in the software. In Table 6.2, it can be seen that the estimated horizontal permeability gives consistent results with the undamaged zone permeabilities used in the simulation indicating that the interpreted horizontal permeability is not affected by the radius of invasion.

For this case study, a negative unit slope indicating the changing in mobility cannot be seen clearly. Since the radius of invasion is too small, the change in mobility can be affected by wellbore storage effect and the spherical flow regime.

In Appendix B, Figure B2 (a), (b), and (c), the regression plots for small radius of invasion (cases K25-50-1, K25-50-2, and K25-50-3) show better consistency on the diagnostic plot than those for large radius of invasion (cases K25-50-4, K25-50-5, and K25-50-6) as shown in Figure B2 (d), (e), and (f). Thus, the regression with vertical interference model can be used very well for small radius of invasion but can be moderately applied for large radius of invasion.

6.2 Case II : Undamaged Permeability of 5 mD, Damaged Permeability of 1 mD

6.2.1 Effects of Mobility Ratio

In this case study, the objective is to investigate the effects of mobility ratio between invaded zone and the reservoir on pressure transients by fixing the permeability of the damaged zone while varying the permeability of the undamaged zone. Three different mobility ratios, K_{hi}/K_{hu} of 0.33, 0.2, and 0.1 are considered. The damaged permeability is fixed at 1 mD while the undamaged permeability varies with mobility ratio. The radius of invasion is fixed at 11.35 ft. away from the borehole wall as shown in Figure 6.8. The flow period consists of a 100-minute drawdown and a 300-minute buildup. After test running of reservoir simulation for pressure response, the data were then interpreted by pressure transient analysis technique. The pressure history and the diagnostic plots of the tests are shown in Figures 6.9 and 6.10, respectively, and the interpreted results are tabulated in Table 6.3. The combination of diagnostic plots of all cases is shown in Figure 6.11. The regression fits to the tests are shown in Appendix B.

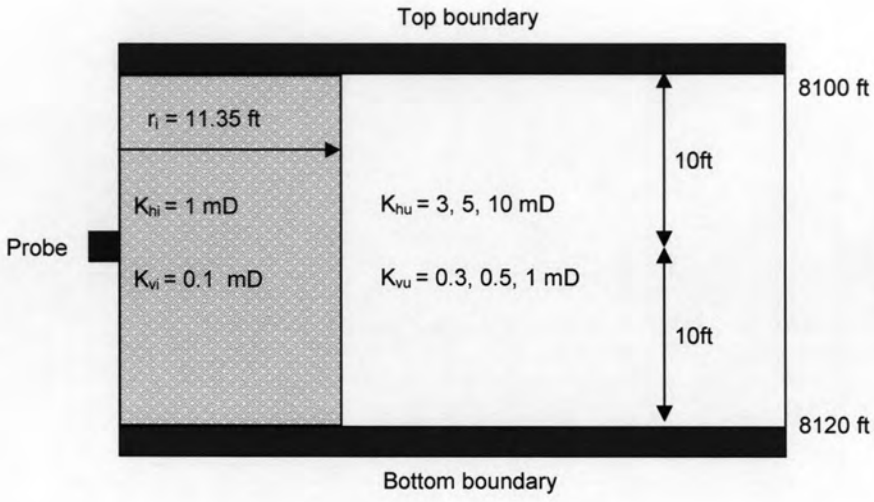

Figure 6.8 : Schematic reservoir description for different mobility ratios between invaded zone and uninvaded reservoir for case II.

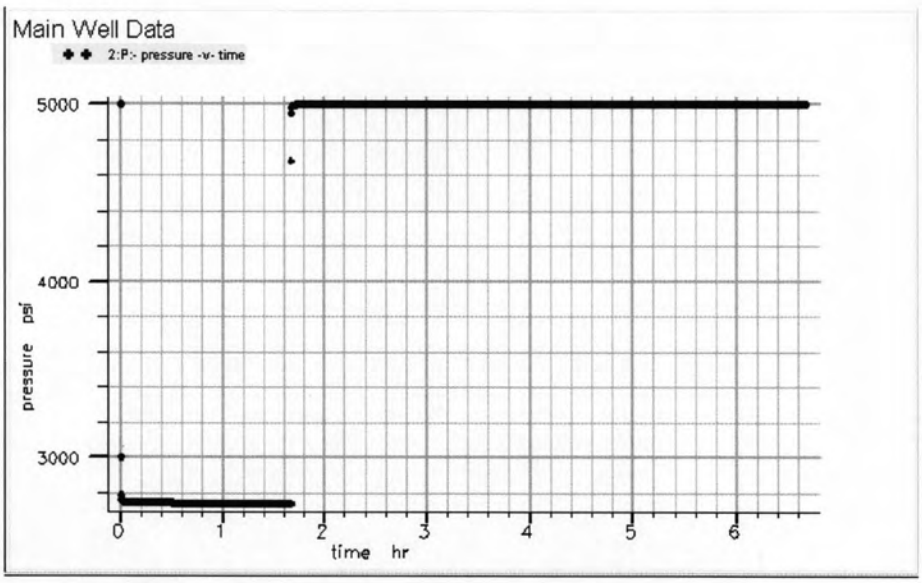

Figure 6.9 : Pressure history of case K1-5 (mobility ratio = 0.2)

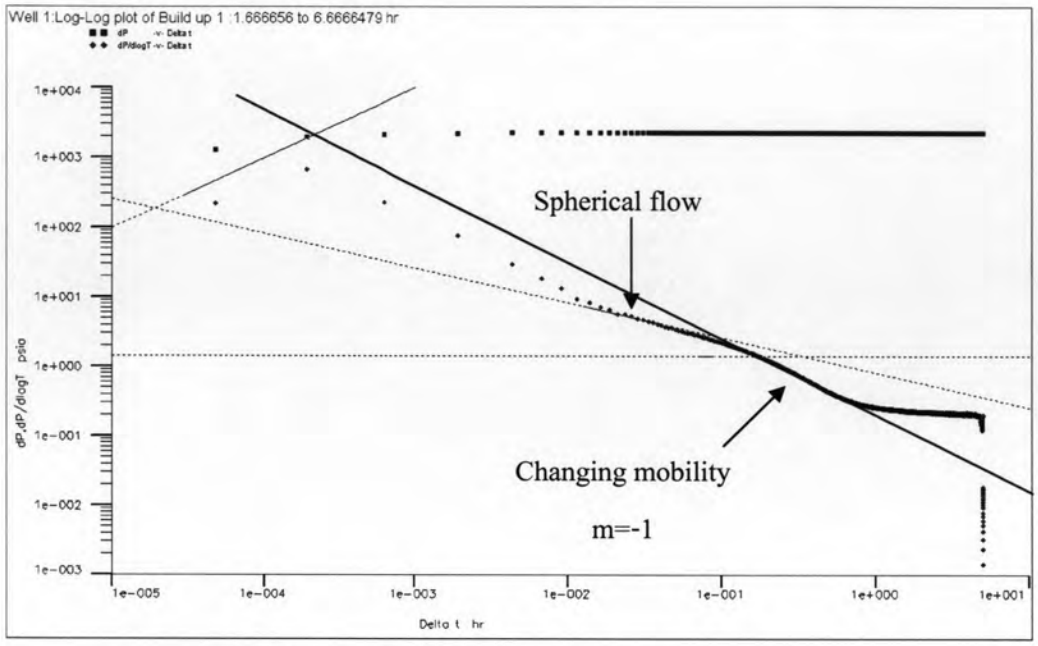

(a)-1 Matched model for inner or damaged zone

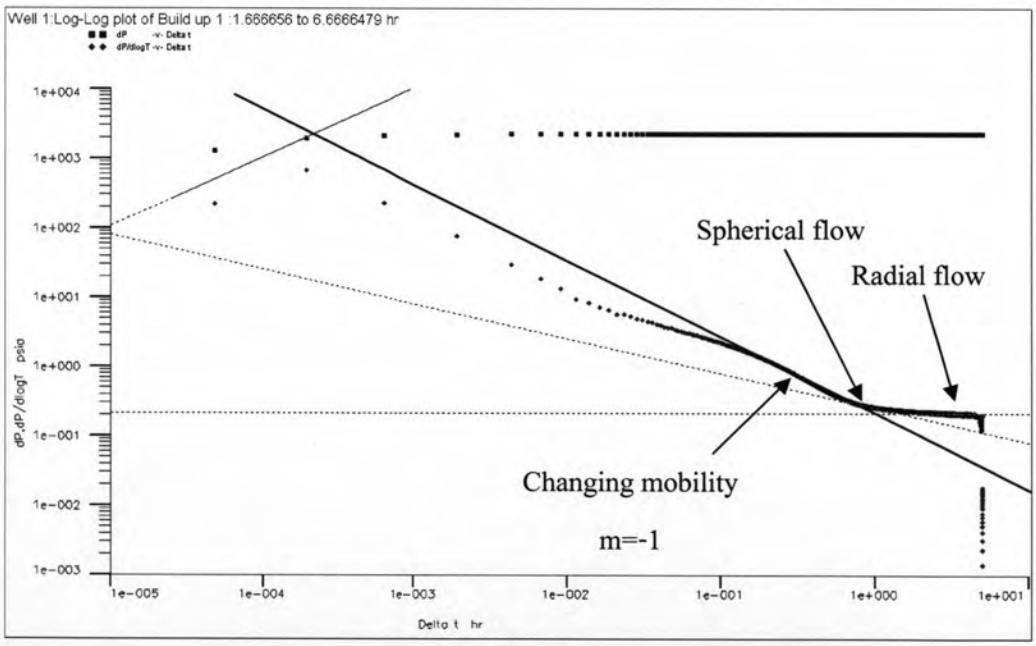

(a)-2 Matched model for outer or undamaged zone

(a) Mobility ratio = 0.333

Figure 6.10 : Diagnostic plots for different mobility ratios between invaded zone and uninvaded reservoir for case II.

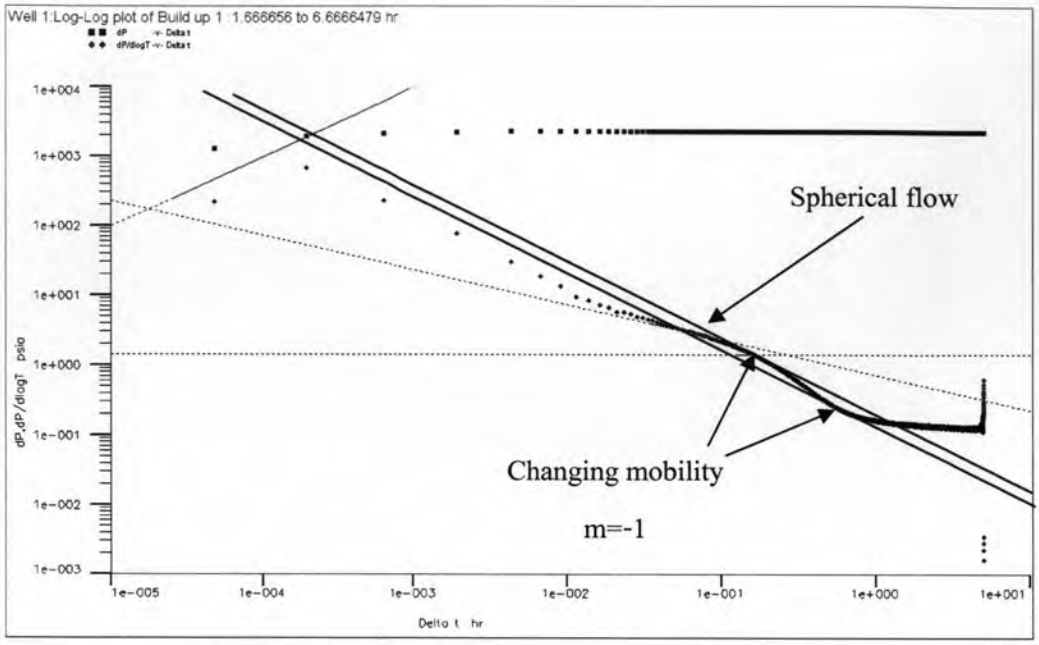

(b)-1 Matched model for inner or damaged zone

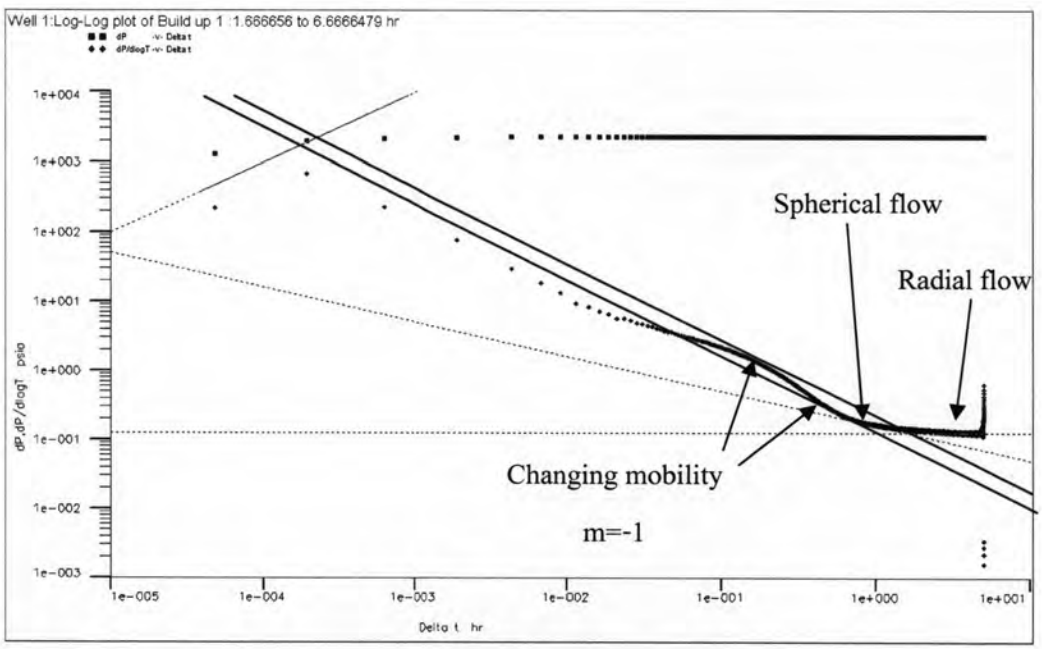

(b)-2 Matched model for outer or undamaged zone

(b) Mobility ratio = 0.2

Figure 6.10 : Diagnostic plots for different mobility ratios between invaded zone and uninvaded reservoir for case II (continued).

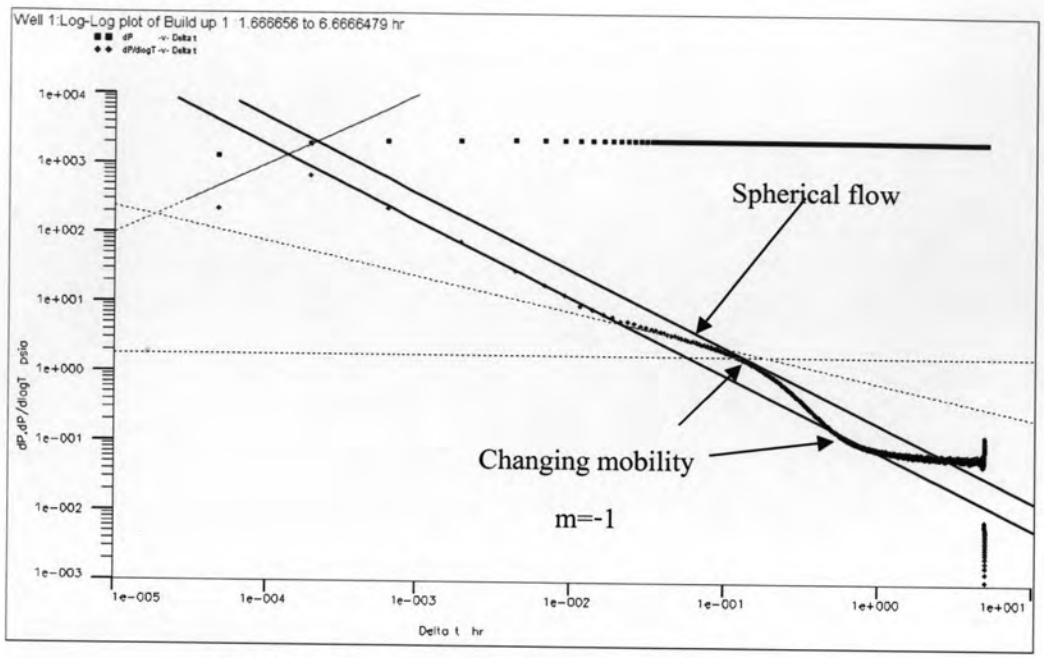

(c)-1 Matched model for inner or damaged zone

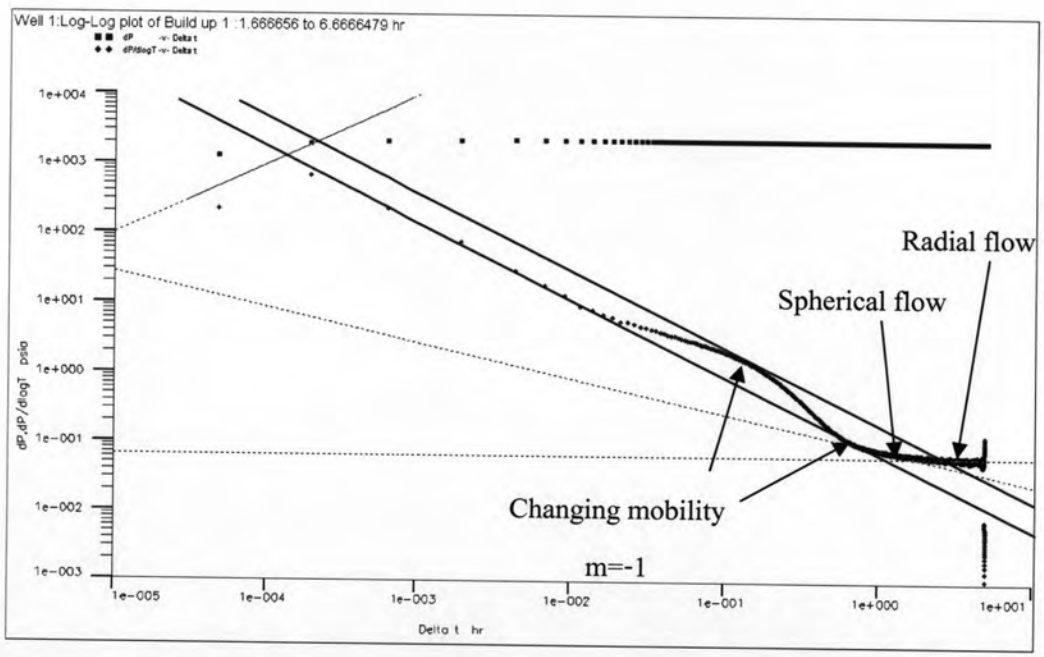

(c)-2 Matched model for outer or undamaged zone

(c) Mobility ratio = 0.1

Figure 6.10 : Diagnostic plots for different mobility ratios between invaded zone and uninvaded reservoir for case II (continued).

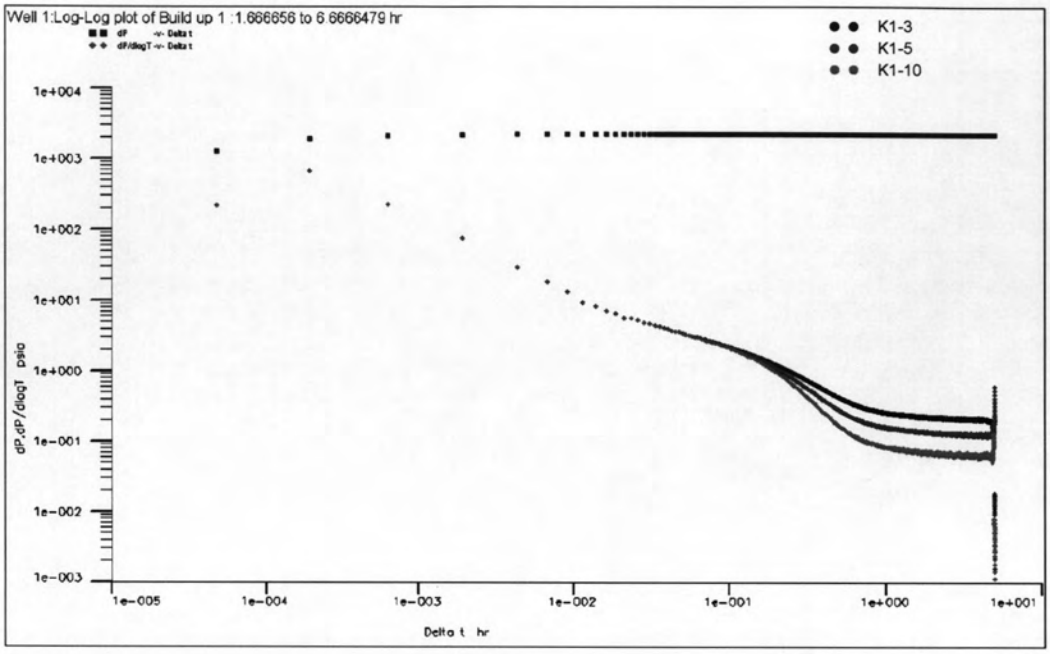

Figure 6.11 : Combination of diagnostic plots for different mobility ratios between invaded zone and uninvaded reservoir for case II.

Table 6.3 : Interpreted results for different mobility ratios between invaded zone and uninvaded reservoir for case II.

Case	K_{hi} (mD)	K_{xyzi} (mD)	K_{hu} (mD)	K_{xyzu} (mD)	S_p	S_M	S_t	Interpreted results				Error %				
								K_{xyzi} (mD)	K_{xyzu} (mD)	K_h (mD)	Skin	K_{xyzi} (mD)	K_{xyzu} (mD)	K_h (mD)	S_M	S_t
K1-3	1	0.464	3	1.392	6.7	7.63	14.33	0.398	0.869	2.68	7.39	-14.22	-37.57	-10.67	-3.14	-48.43
K1-5	1	0.464	5	2.381	6.7	15.26	21.96	0.471	1.192	4.24	7.44	1.50	-19.69	-15.20	-51.24	-66.12
K1-10	1	0.464	10	4.642	6.7	34.34	41.04	0.417	3.848	8.39	7.50	-10.06	-17.10	-16.1	-78.16	-81.73

From the pressure history plot shown in Figure 6.9, the pressure drop is high enough to reduce the noise. So, in this case study, the effect from noise due to too small pressure drop disappears.

As can be seen in the diagnostic plots in Figure 6.10 (a)-1, (b)-1, and (c)-1, the spherical flow model can be matched with the data during the period before changing the mobility to native reservoir mobility. Then, the flow regime changes to spherical flow again corresponding to the outer or undamaged zone. Finally the flow regime becomes radial flow as shown by the model used to match. When increasing the horizontal permeability of the outer zone, the pressure derivative tends to move downward as can be seen in Figure 6.11.

In Appendix B, in Figure B3 (a), (b), and (c), the regressions show inconsistency on log-log diagnostic plot. Since cases K1-3, K1-5, and K1-10 have the radius of invasion of 11.35 ft. which is too large to act like a damaged zone, the reservoir behavior of this case study is similar to that of composite model. But our regression model is simple vertical interference test. Therefore, to make the regression line perfectly match with the data, we need the correct regression model which is single probe with composite reservoir model. However, the required model is not available at this time.

In this case study, we fixed the radius of invasion but varied the permeability in the damaged zone. The effect from the permeability contrast between the native reservoir and the damaged zone can be quantified by the skin factor. The interpreted results for different mobility ratios are summarized in Table 6.3. The spherical permeability and the horizontal permeability are obtained from graphical analysis but the skin factors are obtained from the regression. In cases K1-3, K1-5, and K1-10, the interpreted skin factor is different from the mechanical skin factor calculated from the definition of the skin factor, with an error of -3.14, -51.24, and -78.16 %, respectively. It can be seen that the interpreted skin factors are too small compared with the calculated skin factor and almost the same at 7.50. This is because when we tried to match the regression on the data, the interpreted skin factor cannot be higher than 8.0 or a little more than that. As expressed earlier, the regression model is not the correct model, so the skin factor cannot be interpreted precisely for this case.

In this case study, the radius of invasion is large enough to see the change in mobility, and the spherical permeability of both inner or damaged zone and outer or

undamaged zone can be estimated as summarized in Table 6.3. The interpreted spherical permeabilities of the inner zone are quite similar to the input value but the interpreted spherical permeabilities of the outer zone are much less than the calculated values. This is because the spherical permeabilities obtained from the outer zone are affected by the inner zone. For horizontal permeability, the interpreted results are quite similar to the input value of undamaged zone horizontal permeability suggesting that the interpreted horizontal permeability is not affected by the mobility ratio.

6.2.2 Effects of Radius of Invasion

In this case study, the objective is to investigate the effects of radius of invasion on pressure transients by fixing the permeability of the damaged and the undamaged zone while varying the radius of invasion as depicted in Figure 6.12. Seven different radii of invasions, r_s of 0.44, 0.64, 1.28, 3.35, 4.56, 6.19, and 11.35 ft. are considered. The undamaged permeability is fixed at 5 mD, and the damaged permeability is fixed at 1 mD. The flow period consists of a 100-minute drawdown and a 300-minute buildup. After running reservoir simulation for pressure response, the data were then interpreted by pressure transient analysis technique. The pressure history and the diagnostic plots of the tests are shown in Figures 6.13 and 6.14, respectively, and the interpreted results are tabulated in Table 6.4. The combination of diagnostic plots is shown in Figure 6.15 and the regression fits to the tests are shown in Appendix B.

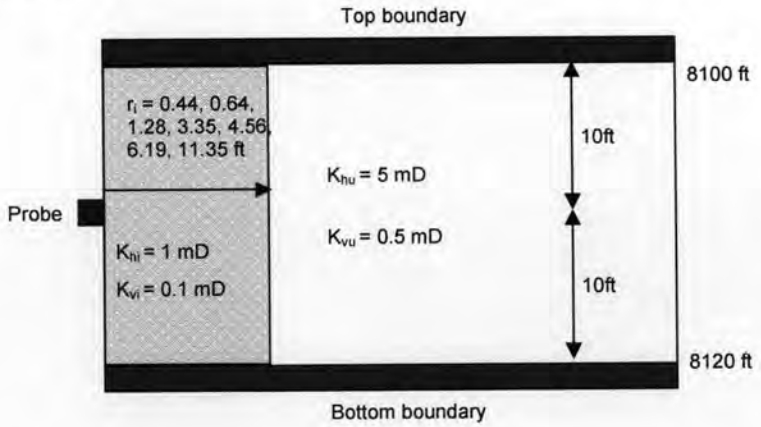

Figure 6.12 : Schematic reservoir description for different radii of invasion for case II.

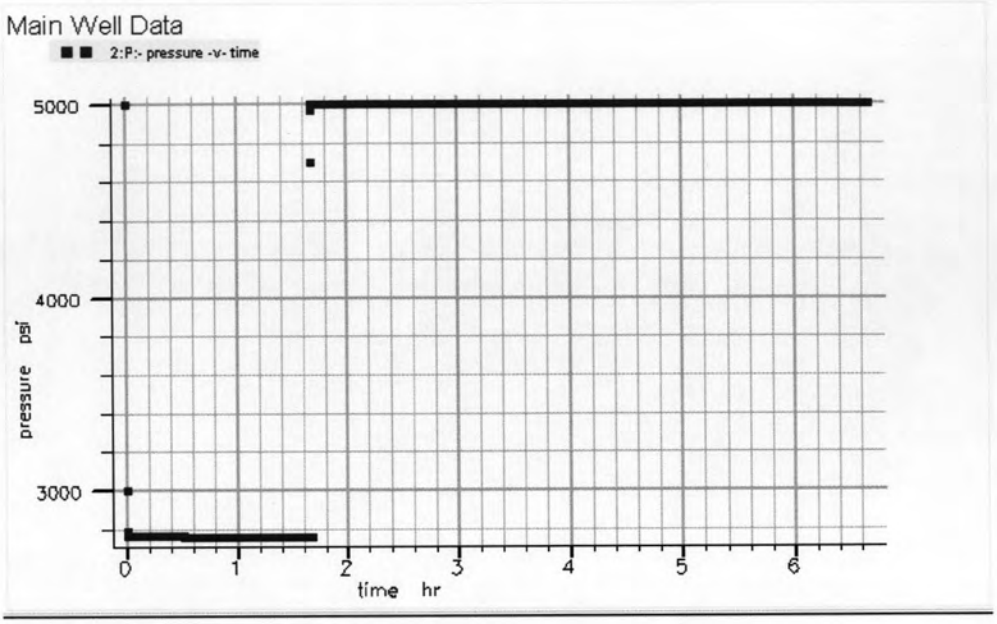

Figure 6.13 : Pressure history for case K1-5-3 (invasion radius = 1.28 ft.)

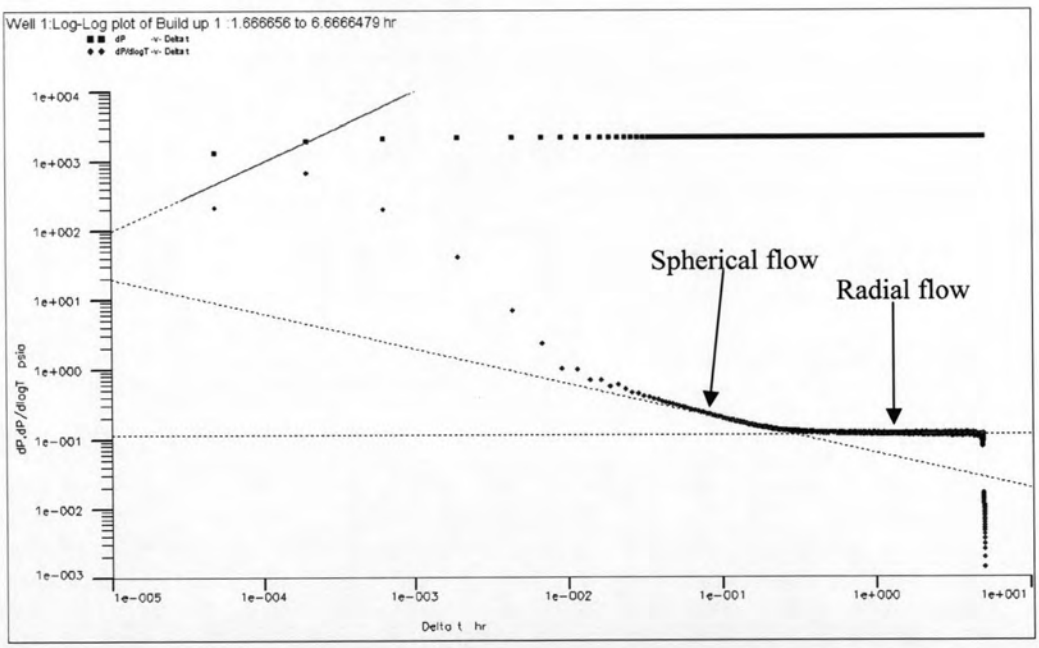

(a) Radius of Invasion = 0.44 ft.

Figure 6.14 : Diagnostic plots for different radii of invasion for case II.

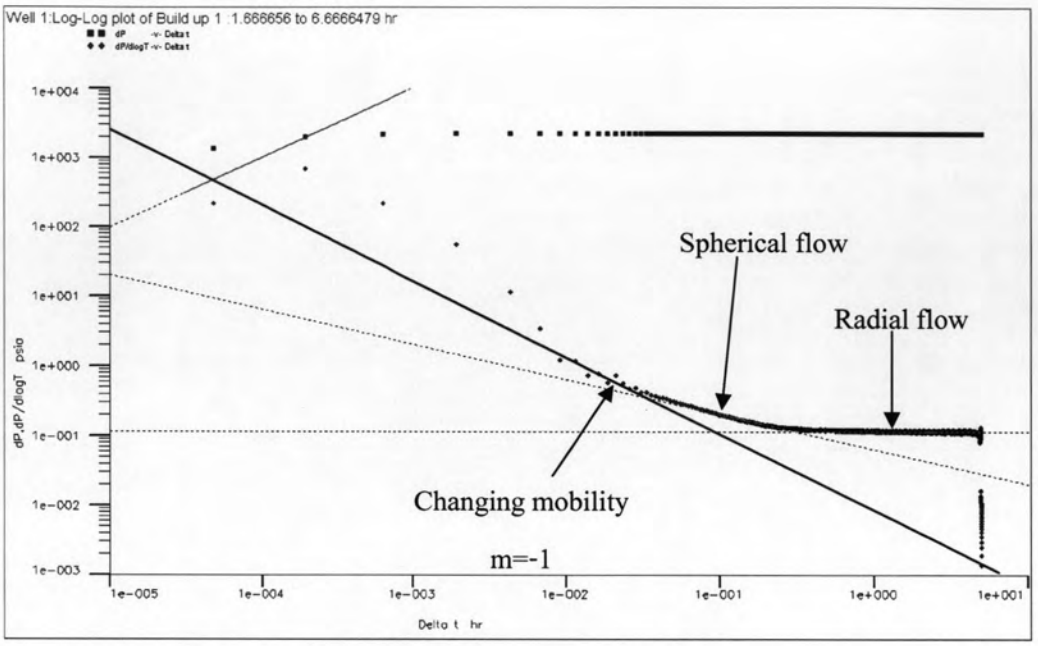

(b) Radius of Invasion = 0.64 ft.

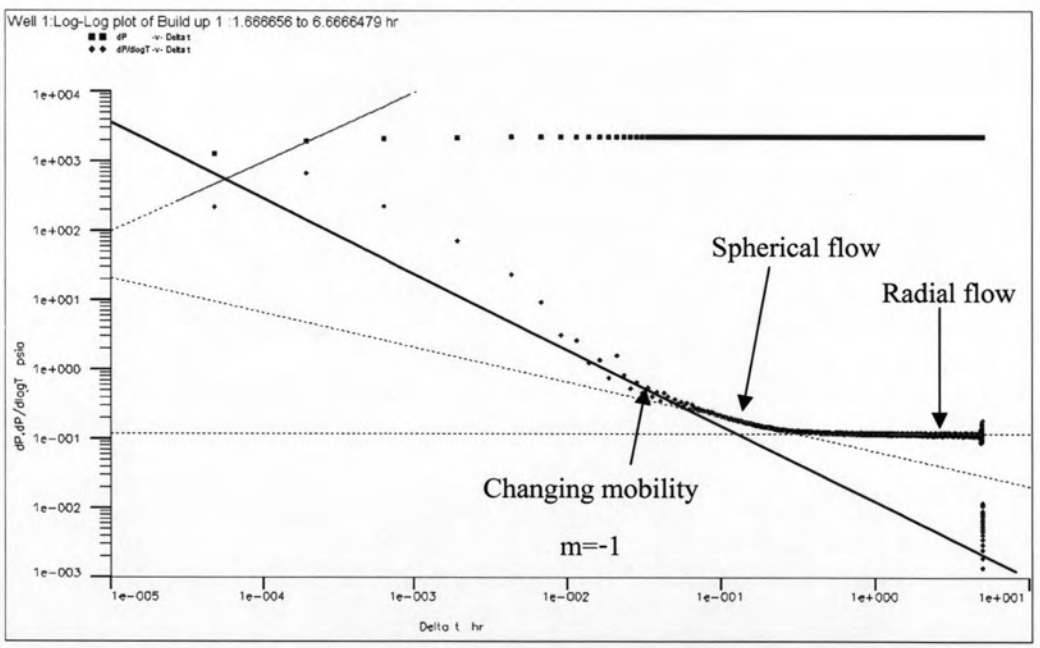

(c) Radius of Invasion = 1.28 ft.

Figure 6.14 : Diagnostic plots for different radii of invasion for case II (continued).

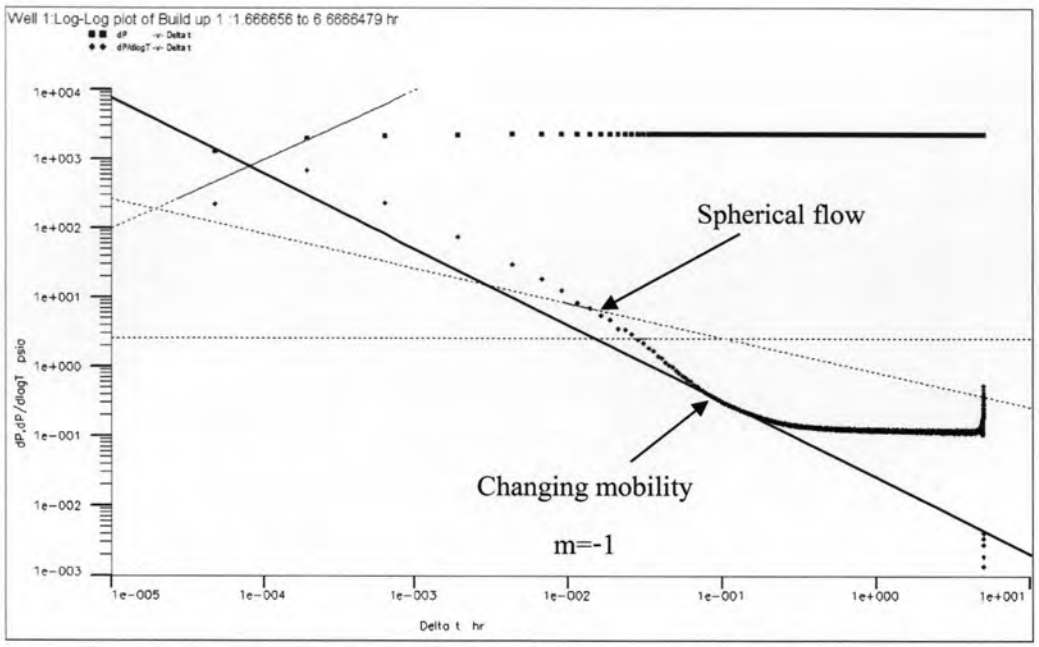

(d)-1 Matched model for inner or damaged zone

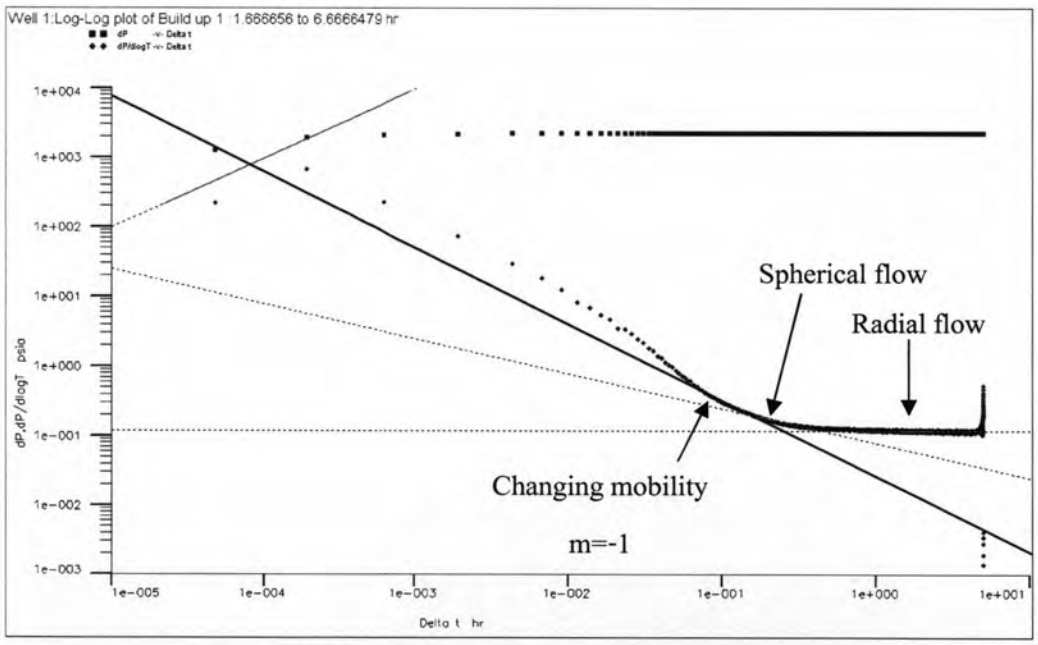

(d)-2 Matched model for outer or undamaged zone

(d) Radius of Invasion = 3.35 ft.

Figure 6.14 : Diagnostic plots for different radii of invasion for case II (continued).

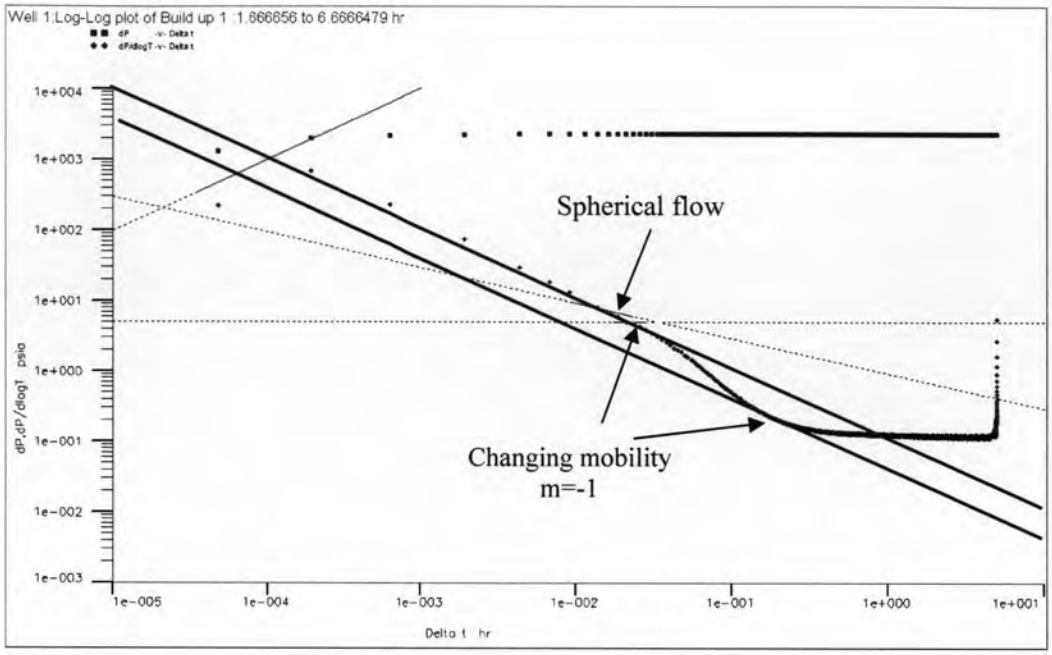

(e)-1 Matched model for inner or damaged zone

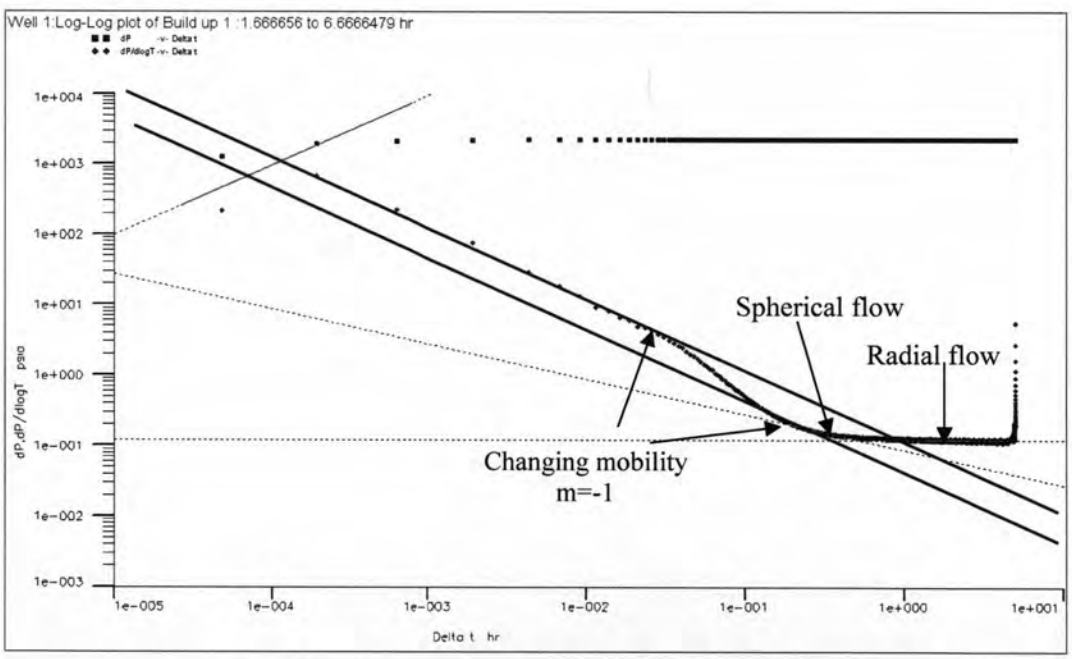

(e)-2 Matched model for outer or undamaged zone

(e) Radius of Invasion = 4.56 ft.

Figure 6.14 : Diagnostic plots for different radii of invasion for case II (continued).

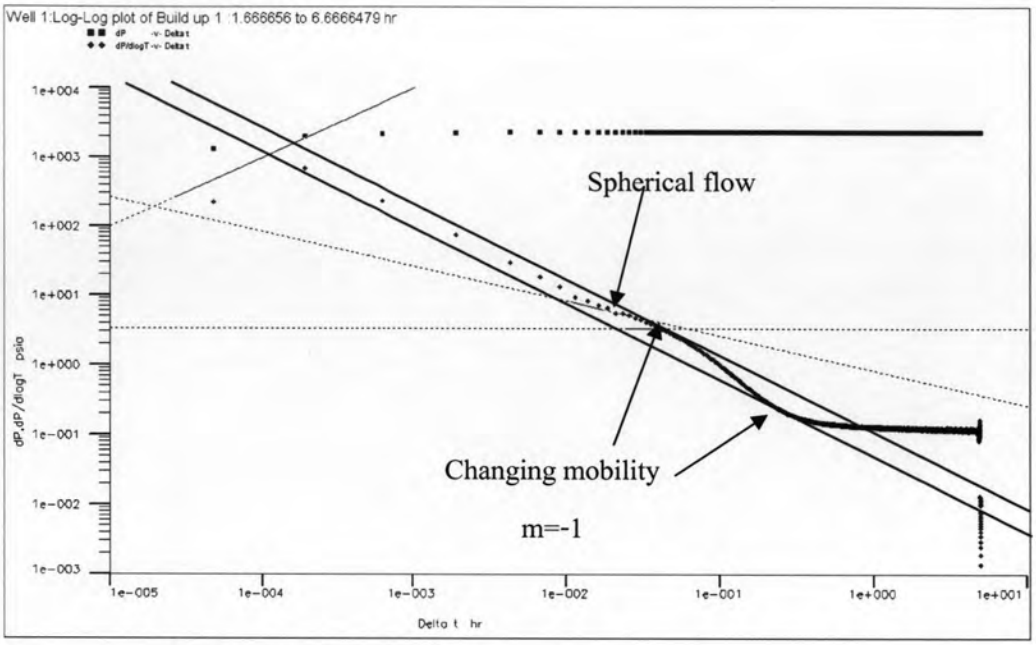

(f)-1 Matched model for inner or damaged zone

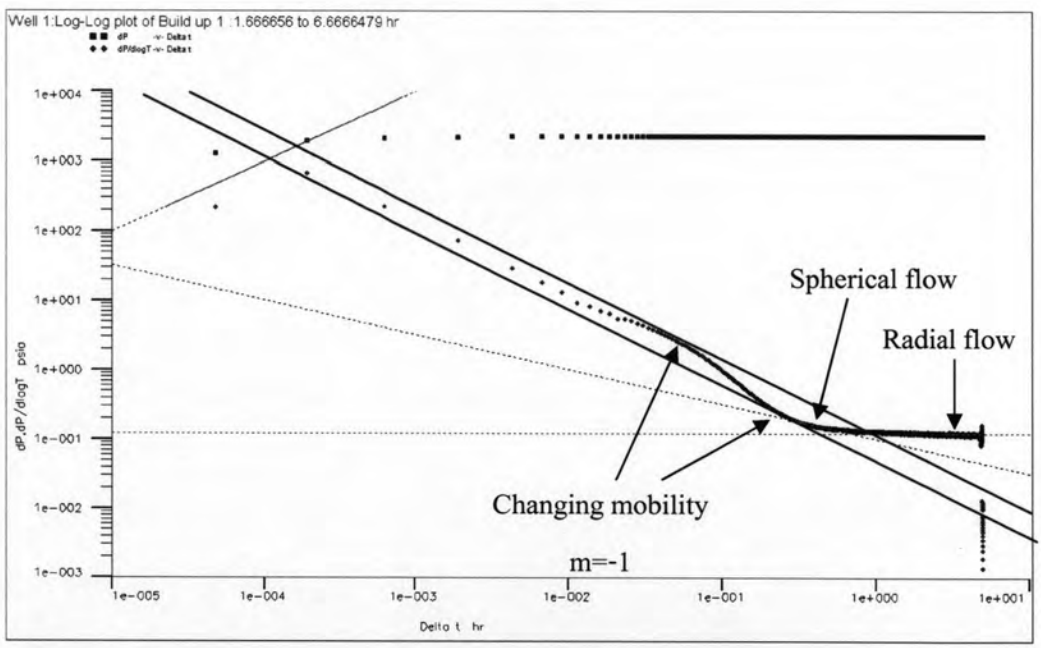

(f)-2 Matched model for outer or undamaged zone

(f) Radius of Invasion = 6.19 ft.

Figure 6.14 : Diagnostic plots for different radii of invasion for case II (continued).

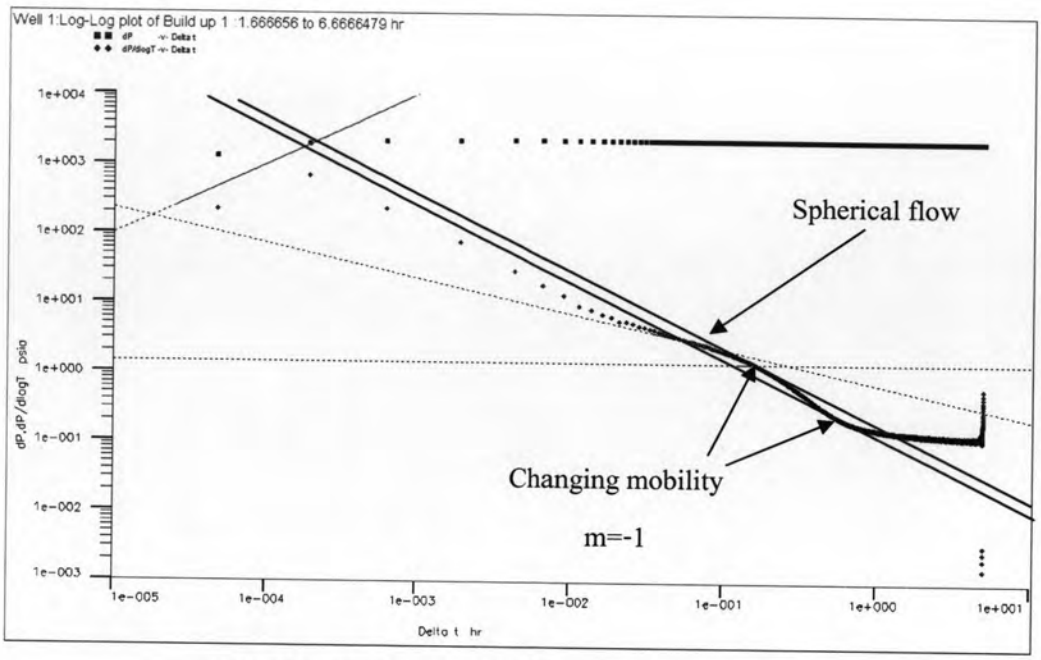

(g)-1 Matched model for inner or damaged zone

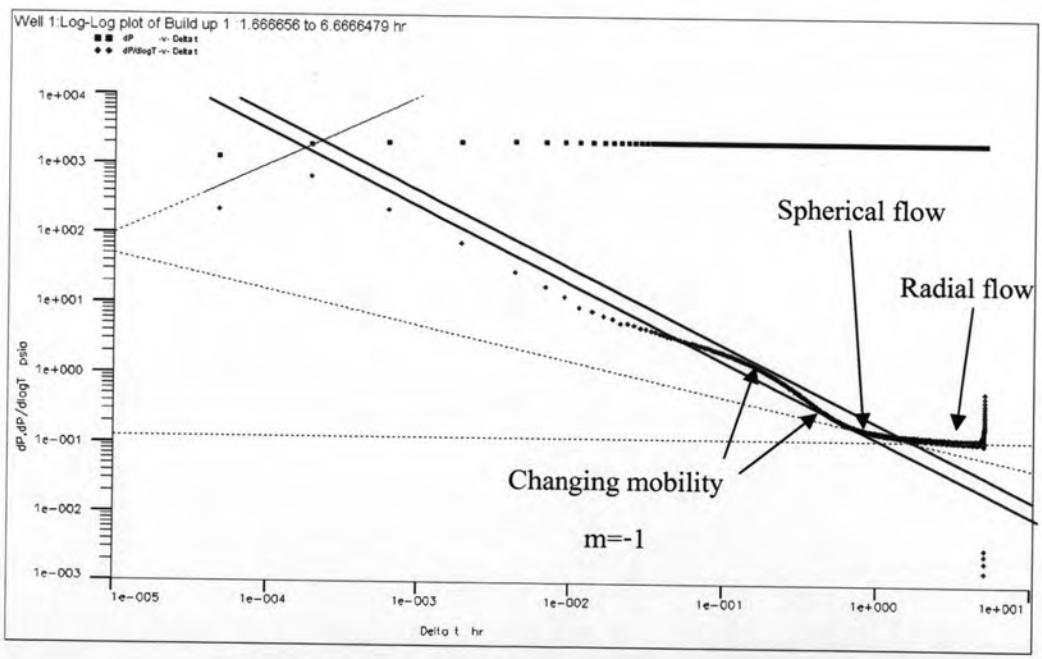

(g)-2 Matched model for outer or undamaged zone

(g) Radius of Invasion = 11.35 ft.

Figure 6.14 : Diagnostic plots for different radii of invasion for case II (continued).

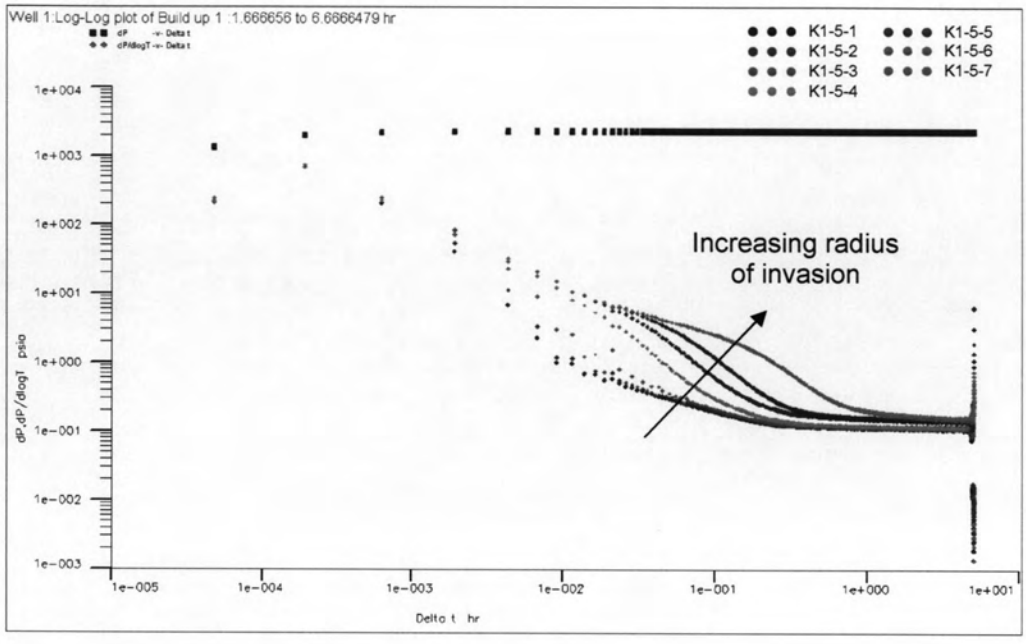

Figure 6.15 : Combination of diagnostic plots for different radii of invasion for case II.

Table 6.4 : Interpreted results for different radii of invasion for case II.

Case	r_s (ft)	K_{hi} (mD)	K_{xyzi} (mD)	K_{hu} (mD)	K_{xyzu} (mD)	S_p	S_M	S_t	Interpreted results				Error %				
									K_{xyzi} (mD)	K_{xyzu} (mD)	K_h (mD)	Skin	K_{xyzi} (mD)	K_{xyzu} (mD)	K_h (mD)	S_M	S_t
K1-5-1	0.44	1	0.464	5	2.321	6.7	2.26	8.96	-	2.219	5.01	8.21	-	-4.39	0.2	263.2	-8.37
K1-5-2	0.64	1	0.464	5	2.321	6.7	3.76	10.46	-	2.193	4.90	7.50	-	-5.51	-2.0	99.47	-28.29
K1-5-3	1.28	1	0.464	5	2.321	6.7	6.53	13.23	-	2.121	5.08	7.89	-	-8.61	1.6	20.82	-40.36
K1-5-4	3.35	1	0.464	5	2.321	6.7	10.38	17.08	0.395	1.898	4.93	7.75	-14.87	-18.22	-1.4	-25.34	-54.62
K1-5-5	4.56	1	0.464	5	2.321	6.7	11.61	18.31	0.411	1.780	4.72	7.07	-11.42	-23.31	-5.6	-39.10	-61.38
K1-5-6	6.19	1	0.464	5	2.321	6.7	12.83	19.53	0.397	1.602	4.79	7.4	-14.44	-30.97	-4.2	-42.32	-62.10
K1-5-7	11.35	1	0.464	5	2.321	6.7	15.26	21.96	0.471	1.192	4.24	7.4	1.51	-48.64	-15.2	-51.51	-66.30

From the pressure history plot shown in Figure 6.13, the pressure drop is high enough to reduce the noise. So, in this case study, the effect from noise due to too small pressure drop goes away.

As can be seen in the diagnostic plots of large radius of invasion cases shown in Figure 6.14 (d)-1 to (g)-1, the spherical flow model can be matched with the data during the early period. Then, the flow regime changes to spherical flow again corresponding to the outer or undamaged zone. Finally, the flow regime becomes radial flow as shown by the matched model in Figure 6.14 (g)-2 to (g)-2. For small radius of invasion cases as shown in Figure 6.14 (a), (b), and (c), the spherical flow of the inner or damaged zone and the change in mobility cannot be seen apparently. This is because the radius of invasion is too small, so the flow regimes of the inner zone are influence by wellbore storage effect. When increasing the radius of invasion, the pressure derivative tends to move upward as can be seen in Figure 6.15.

In Appendix B, in Figure B4 (a) and (b), the regression plots of low radius of invasion (cases K1-5-1 and K1-5-2) show better consistency on the diagnostic plot than those for large radius of invasion (cases K1-5-3, K1-5-4, K1-5-5, K1-5-6 and K1-5-7) as shown in Figure B4 (c)-(g). This is because when the radius of invasion is too large, the reservoir behavior is similar to that of a composite model but the regression model is vertical interference test. Thus, the regression with vertical interference model can be moderately applied in the case of small radius of invasion but cannot be used in the case of large radius of invasion. In order to make the regression perfectly match with the data, we need the correct regression model which is a single probe with composite reservoir model. However, the required model is not available at this time.

The interpreted results for different radii of invasion are summarized in Table 6.4. The spherical permeability and the horizontal permeability are obtained from graphical analysis but skin factors are obtained from the regression. It can be seen that the interpreted skin factor of case K1-5-1 is overestimated compared with the mechanical skin, S_M. This is due to the fact that the interpreted skin factor is affected by the spherical skin or the skin due to probe, S_P as can be seen that the error between the interpreted result and the total skin factor, S_t is reduced to -8.37 %. For cases K1-5-4, K1-5-5, K1-5-6 and K1-5-7 which have large radius of invasion, the interpreted skin factor are underestimated compared with the mechanical skin factor, S_M and

almost the same at 7.5. This is because when we tried to match the regression on the data, the interpreted skin factor cannot be higher than 8.0 or a little more than that. As expressed earlier, the regression model is not correct model, so the skin factor cannot be interpreted precisely for this case.

In this case study, for small radius of invasion, cases K1-5-1, K1-5-2, and K1-5-3, the spherical permeability of the inner zone cannot be estimated but for large radius of invasion, cases K1-5-4, K1-5-5, K1-5-6, and K1-5-7, the radius of invasion is large enough to see the change in mobility, and the spherical permeabilities of both the inner or damaged zone and the outer or undamaged zone can be determined. From Table 6.4, the interpreted spherical permeabilities of the inner zone are quite similar to the input value but the interpreted spherical permeabilities of the outer zone are much less than the calculated value. The error increases when the radius of invasion increases. This is because the spherical permeability obtained from the outer zone is affected by the inner zone. For horizontal permeability, the interpreted results are quite similar to the input value of undamaged zone horizontal permeability indicating that the interpreted horizontal permeability is not affected by the radius of invasion.